AGU ADVANCING EARTH AND SPACE SCIENCE

Geophysical Research Letters®

RESEARCH LETTER
10.1029/2022GL098402

Across-Slab Propagation and Low Stress Drops of Deep Earthquakes in the Kuril Subduction Zone

Alice R. Turner[1], Ana M. G. Ferreira[2,3], Andrea Berbellini[3,4], Nicolas Brantut[3], Manuele Faccenda[5], and Elodie Kendall[6]

[1]Department of Earth Sciences, University of Oxford, Oxford, UK, [2]CERIS, Instituto Superior Técnico, Universidade de Lisboa, Lisbon, Portugal, [3]Department of Earth Sciences, University College London, London, UK, [4]Istituto Nazionale di Geofisica e Vulcanologia, Sezione di Bologna, Bologna, Italy, [5]Dipartimento di Geoscienze, Università di Padova, Padua, Italy, [6]GFZ German Research Centre for Geosciences, Potsdam, Germany

Key Points:

- Seismic inversion of deep earthquake properties shows low stress drops and high radiation efficiency
- Comparison with thermal models shows that events are mostly confined to regions with temperatures lower than 1,000°C
- The same physics may control the propagation of deep and shallow earthquakes

Supporting Information:

Supporting Information may be found in the online version of this article.

Correspondence to:

A. R. Turner,
alice.turner@earth.ox.ac.uk

Citation:

Turner, A. R., Ferreira, A. M. G., Berbellini, A., Brantut, N., Faccenda, M., & Kendall, E. (2022). Across-slab propagation and low stress drops of deep earthquakes in the Kuril subduction zone. *Geophysical Research Letters*, *49*, e2022GL098402. https://doi.org/10.1029/2022GL098402

Received 25 FEB 2022
Accepted 11 AUG 2022

Abstract Deep earthquakes occur down to 700 km depth where pressure is up to two orders of magnitude greater than in the crust. Rupture characteristics and propagation mechanisms under those extreme conditions are still poorly constrained. We invert seismic waveforms for the spatial dimensions, duration and stress drop of deep-focus earthquakes (M_w 6.7–7.7) in the Kuril subduction zone. We find stress drops of ∼1–10 MPa and rigidity-corrected spatial dimensions and durations similar to crustal earthquakes. Radiated efficiency >1 is observed, suggesting that undershooting is prevalent in deep earthquakes, consistent with laboratory derived weakening mechanisms. Comparisons with subduction models suggest across-slab propagation within regions with temperatures $T < \sim 1{,}000$°C, similar to shallow events. Hence, despite different triggering mechanisms, the same physics seems to control the rupture propagation of both shallow and deep earthquakes.

Plain Language Summary Deep earthquakes occur where subducting slabs dive into the mantle at depths of up to 700 km, where high pressures and temperatures should prevent the occurrence of earthquakes. It is not clear how deep earthquakes start or propagate under these conditions. We consider eight earthquakes in the Kuril subduction zone and estimate their properties. After correcting for the way material properties vary with depth, we find that these deep earthquakes have similar durations, spatial extents, and stress drops as shallow (<70 km) earthquakes. When we compare the earthquake spatial extents to thermal models, we find these deep earthquakes are confined to the coolest part of the slab. These findings suggest that the same physics may control the propagation of deep and shallow earthquakes.

1. Introduction

Earth's evolution is ultimately driven by convection in its deep interior. In turn, subduction is the main engine of convection. As oceanic lithosphere plunges into the Earth, it creates high stresses, transports water and volatiles into the mantle, and goes through phase transformations. Subduction zones are the locus of some of the largest, destructive earthquakes on Earth, which mainly occur at shallow depths. As depth increases (>70 km) the confining pressures are so large that they should inhibit frictional sliding. Yet, 25% of all earthquakes in seismic catalogs are intermediate- (70 < depth <300 km) and deep-focus (depth > 300 km) events (Houston, 2015). For simplicity, in the remainder of this paper we will refer to intermediate- and deep-focus events as deep earthquakes. The main hypotheses proposed for the initiation and propagation mechanisms of deep earthquakes are: (a) Transformational faulting (or anti-crack faulting), which proposes that metastable olivine is transported into the transition zone (at ∼410–660 km depth) in the high stress, very cold slab core, defining a metastable olivine wedge (MOW), where its transformation to wadsleyite and ringwoodite leads to faulting and earthquakes (Kirby et al., 1996; Wang et al., 2017), (b) Thermal runaway, where heterogeneity in the host rock leads to the formation of a plastic instability, shear heating, the localization of strain and a runaway shear melting process (Ogawa, 1987) and, (c) Dehydration embrittlement, whereby the decomposition of hydrous phases or partial melting of carbonates increases locally the pore fluid pressure, which allows brittle failure to occur at greater depths than would normally be possible (Davies, 1999). Moreover, two or more deep earthquake mechanisms may operate together (Zhan, 2019). In addition to the mechanism that triggers deep earthquakes, the differences between the rupture properties of deep and shallow earthquakes are also debated and up to now it has been unclear whether deep and shallow events are controlled by the same rupture physics (Houston, 2015). Constraining the

physics of deep earthquakes is important for understanding the stress, thermal state and fate of subducted slabs, subduction dynamics and mantle convection.

Due to the great depth of the events, seismology is the main way to study deep earthquakes. However, the detection and unambiguous description of deep earthquake ruptures are challenging because they occur far from seismic stations. A range of different seismic methods have previously been applied to determine the source of deep-focus earthquakes; for example, durations can be determined from the stacking of high-frequency P-waves (Houston et al., 1998; Poli et al., 2016), source time functions (Campus & Das, 2000), or corner frequency approaches (Liu et al., 2020; Poli & Prieto, 2014). Similarly, detailed studies of the geometry, spatial dimensions and complex slip histories combine multiple methods, often utilizing high-frequency data. Common methods include directivity and sub-event analyses (Zhan et al., 2014), distributed seismic slip inversions and back-projection techniques (Ye et al., 2013), and detailed analysis of P-waves (Ruiz et al., 2017). Yet, the different modeling approaches, assumptions and constraints utilized in different studies of the same event often lead to large variations in estimates of source properties, sometimes by a factor of two or more (Ruiz et al., 2017; Wei et al., 2013; Ye et al., 2013; Zhan et al., 2014). These methods have provided a wealth of information of individual deep earthquakes; however, because of the variation in estimates of source properties, comparative studies remain a challenge.

Previous studies comparing the rupture properties of deep earthquakes have shown that these events generally have a shorter duration and are more spatially compact than shallow events with the same magnitude (Houston, 2015). The picture is less clear for other source properties. For instance, static stress drop—the difference between the shear stress on the fault before and after the earthquake—is a source parameter that holds important information about the physics of the rupture. It is given by

$$\Delta\sigma = c\mu u / S^{1/2}, \tag{1}$$

where μ is the rigidity, u is the average slip, S is the source area, and c is a constant $\sim$1 determined mainly by the fault's geometry (Eshelby, 1957). While Liu et al. (2020) report mean stress drops of deep earthquakes to be an order of magnitude larger than shallow earthquakes, Poli et al. (2016) found stress drops of 95% earthquakes with depths of 400–700 km to 3.6–49.2 MPa, similar to shallow crustal events.

In addition, whilst some studies report a depth dependence in source properties which may be linked to a change in mechanism between intermediate- and deep-focus earthquakes (Liu et al., 2020; Vidale & Houston, 1993), others have shown no such dependency (Campus & Das, 2000) or found that the apparent increase of stress drop with depth can be explained by the increase of rigidity (Vallée, 2013). To further explore the behavior of deep earthquakes, in this study, we use a second-degree moments technique (Backus, 1977a, 1977b; Clévédé et al., 2004; McGuire et al., 2001) to find robust characteristic values of source parameters of deep events in the Kuril subduction zone. The second-degree method makes few assumptions about the geometry of the rupture, and none about the rupture velocity. Although only providing a "low-resolution" image of bulk seismic source, lacking the spatial-temporal complexity highlighted by higher frequency methods, the second-degree moments method provides a simple, robust, and easily interpretable description of deep earthquakes.

The Kuril subduction zone is relatively simple, with a fairly planar slab (Fukao & Obayashi, 2013), which reduces the effect of slab complexities on the rupture properties (Fan et al., 2019; Ye et al., 2016). In this region, the Pacific plate subducts beneath the Sea of Okhotsk at a rate of around 7 cm/yr. The Kuril slab is old, with an estimated age of $\sim$106–109 Ma and a $\sim$45 km thick Wadati-Benioff zone (Syracuse & Abers, 2006). Throughout most of the subduction zone, the slab dip is between 46° and 50° (Syracuse et al., 2010). In the northern part of the subduction zone, the slab penetrates to the lower mantle, while in the south, the slab flattens above the 660 km seismic discontinuity (Fukao & Obayashi, 2013), creating a gentle hinge that influences the earthquake focal mechanisms (Myhill, 2012). Seismicity occurs throughout the slab, with the deepest events occurring in the north down to >600 km. Previous seismological studies reported that intermediate depth earthquakes in the region tend to rupture on a sub-horizontal fault plane (Warren et al., 2015), following trends observed in other subduction zones (Antolik et al., 1999; Kiser et al., 2011; Warren et al., 2007, 2008).

Moreover, the Kuril subduction zone produced the largest magnitude deep focus earthquake on record—the 24 May 2013 M_w 8.3 Okhotsk earthquake at 611 km depth (Steblov et al., 2014). Several studies analyzed this significant event (Chen et al., 2014; Meng et al., 2014; Park & Ishii, 2015; Wei et al., 2013; Ye et al., 2013, 2016),

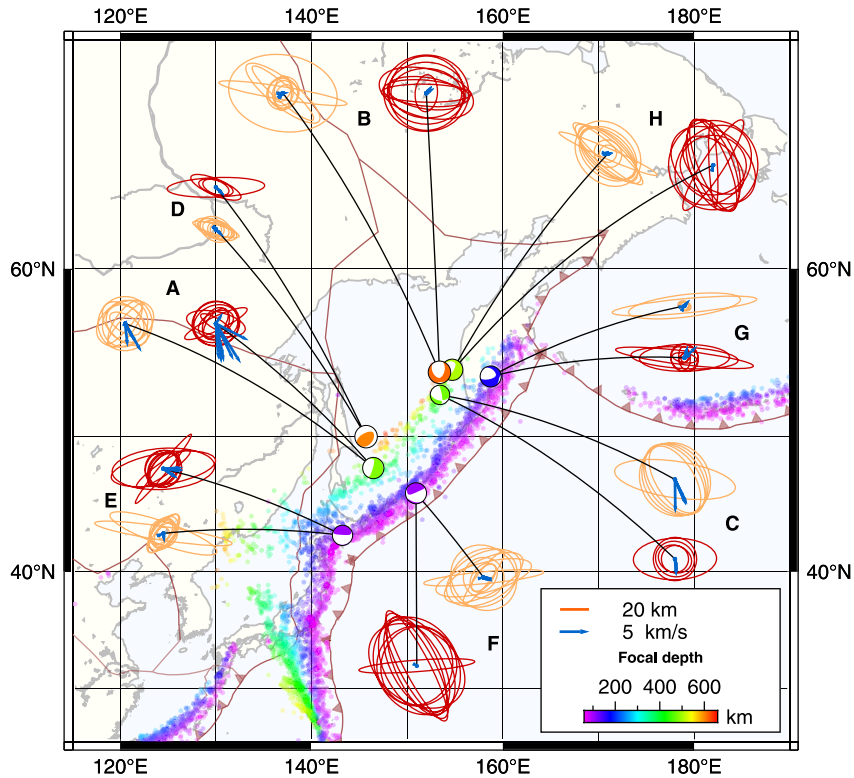

Figure 1. Map view of the eight deep earthquakes investigated in this study (events A–H, see the corresponding source parameters in Table S1 in the Supporting Information S1) in the Kuril subduction zone. The events are indicated by their associated focal mechanism, scaled to the magnitude of the event and colored by focal depth. The ellipses represent the range of 20 best-fitting maximum (A_{max}) and minimum (A_{min}) characteristic source dimensions and Φ values for each event found in this study (orange and red ellipses were obtained assuming sub-vertical and sub-horizontal fault planes, respectively). The blue arrows show the centroid velocity vectors (v_0) obtained in this study. Plate boundaries are marked in brown. Background seismicity from EHB data (Engdahl et al., 1998) with an upper bound of 60 km are shown, colored by focal depth.

leading to estimates of the maximum spatial extent ranging from 64 km (Chen et al., 2014) to 180 km (Ye et al., 2013), with stress drops varying from 8 MPa (Wei et al., 2013) to 15 MPa (Ye et al., 2013) and fast rupture speeds of 4–4.5 km/s (Wei et al., 2013; Ye et al., 2013). The large variability in these seismic solutions despite the data's good signal-to-noise ratio highlights the non-uniqueness of the approaches typically used in source inversions, particularly when applied to deep earthquakes.

2. Seismic Modeling

In this study we investigate eight M_w 6.7–7.7 deep earthquakes with ~100–600 km depth in the Kuril subduction zone that occurred between 2002 and 2018 (Figure 1, Table S1 in the Supporting Information S1). We use a second-degree moments inversion technique (Clévédé et al., 2004; McGuire et al., 2001), which involves calculations of second-degree central moments of moment tensor density (stress glut) to directly invert seismic body waveforms for the events' spatial dimensions (characteristic fault length and width, A_{max} and A_{min}), rupture duration and speed, along with their uncertainties (Figure S1 in the Supporting Information S1). We use full waveform modeling combining the 3-D global crust model CRUST2.0 (Bassin, 2000) with the 3-D mantle model SGLOBE-rani (Chang et al., 2015), and perform inversions with a Monte Carlo algorithm (Sambridge, 1999). For each earthquake we perform inversions successively varying the A_{min}/A_{max} ratio between 0.1 and 1.0 with steps of 0.1. We fix the moment magnitude and two possible fault planes to the Global Centroid Moment-Tensor (GCMT) solution, and impose $A_{min} > 5$ km to stabilize the inversions (see full method details in the Supporting Information S1). Hence, we perform 20 different source inversions for each earthquake.

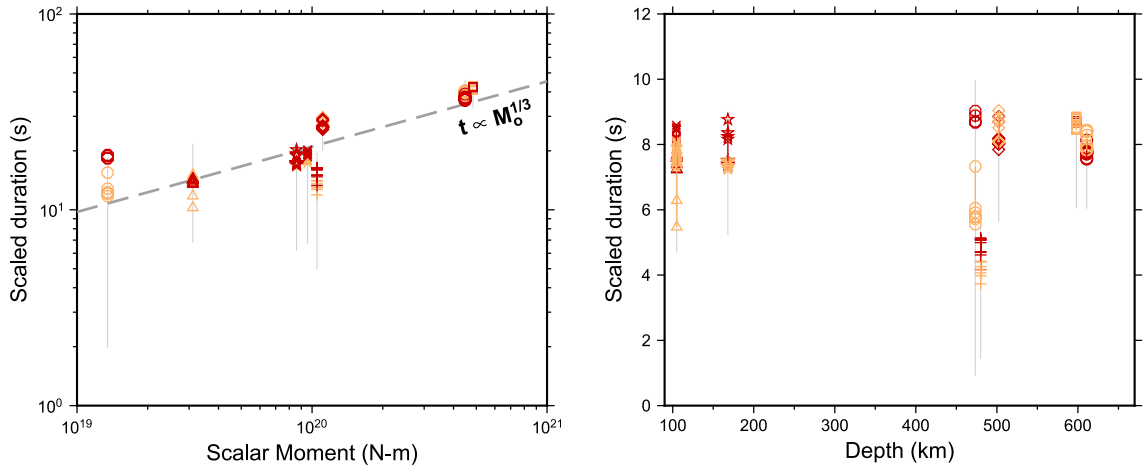

Figure 2. Left: Best-fitting source durations determined in this study from the 20 different source inversions performed for each earthquake and corrected by the rigidity at the source's depth (see Figure S43 in Supporting Information S1 for the unscaled durations obtained in this study). The corrected durations follow the $t \propto M_0^{1/3}$ relation valid for shallow earthquakes (Ekström et al., 2012). Each event is represented by a different symbol (A: plus; B: circle; C: diamond; D: star; E: triangle; F: cross; G: octagon; H: square; see the corresponding source parameters in Table S1 in the Supporting Information S1). Orange and red symbols correspond to solutions obtained assuming sub-vertical and sub-horizontal fault planes, respectively. Right: Scaled source duration as a function of depth, showing no depth dependency. Gray lines in both panels show model uncertainty, determined from all models within 5% of the minimum misfit.

From the earthquake's spatial dimensions and using the seismic moment reported in the GCMT catalog we estimate the static stress drop $\Delta\sigma$ using Equation 1. We can gain additional information about the physics of rupture from earthquake source time functions. These source time functions describe the variation of the moment rate with time, which is not recovered by spatially and temporally averaged properties of the overall rupture process determined by using second degree moments. As such, we use published source time functions from the SCARDEC catalog (Vallée & Douet, 2016; Vallée et al., 2011), which provide complementary information to this study. Using high-frequency non-smoothed source time functions of the events from the SCARDEC catalog we estimate the radiated energy (E_R) by integrating the source time function (e.g., Bilek et al., 2004; Chounet & Vallée, 2018; Denolle, 2019; Vassiliou & Kanamori, 1982). The radiated energy is then used together with the stress drop and seismic moment to estimate the apparent radiation efficiency (Venkataraman & Kanamori, 2004):

$$\eta_{app} = 2\mu E_R / (\Delta\sigma_s M_0)\,. \tag{2}$$

Although the stress drop may be determined from the duration of the source time function using an assumed rupture velocity (Courboulex et al., 2016; Vallée, 2013), we choose to use the stress drops we determine directly from the spatial extents. The radiated energy and efficiency are key properties of earthquakes, which give additional information about deep earthquake physics, the similarities between shallow and deep earthquakes, and their mechanisms.

Overall the source durations determined in this study are well constrained, having good data coverage (Figures S6, S12, S16, S20, S24, S28, S32, and S36 in Supporting Information S1) and showing excellent data fits (Figures S7, S8, S13, S14, S17, S18, S21, S22, S25, S26, S29, S30, S33, S34, S37, and S38 in Supporting Information S1) and a sharp convergence (Figures S9, S15, S19, S23, S27, S31, S35, and S39 in the Supporting Information S1), and agree well with those estimated from source-time functions from the SCARDEC catalog (Figure S43 in Supporting Information S1, Vallée et al., 2011; Vallée & Douet, 2016). In some cases our estimates of duration are shorter than those obtained from the source time functions by ~1–7 s, which is likely due to complexity in the later part of the source process that is not captured by our analysis or to minor artefacts in the source time functions resulting from the deconvolution (e.g., Earth structure effects). The estimated source durations Δt determined in this study are ~45% shorter than those obtained using the duration-magnitude scaling law employed by the GCMT catalog (Ekström et al., 2012), which is valid for shallow earthquakes (Figure 2). This is equivalent to a change in the exponent of the magnitude-duration scaling from $\Delta t \propto M_0^{\frac{1}{3}}$ to $\Delta t \propto M_0^{0.21}$, similar to findings from previous studies (Campus & Das, 2000; Houston et al., 1998; Poli & Prieto, 2014). The scaled durations calculated using Equation 6 in the Supporting Information S1 do not show a depth dependency (Figure 2), in

agreement with some previous studies (Poli & Prieto, 2014; Vallée, 2013). When scaling our durations by the rigidity at the source depth, we find that our duration estimates agree well with the $\Delta t \propto M_0^{\frac{1}{3}}$ scaling law for shallow events (Figure 2). This shows that the differences in duration between the deep earthquakes investigated in this study and shallow events can be explained by the change of rigidity with depth.

The two reported GCMT fault planes lead to very similar data misfits and thus we are unable to identify a preferred fault plane based on data fit. Figure 1 shows the source spatial dimensions obtained for the events studied assuming both sub-horizontal and sub-vertical fault planes. Despite some scattering in the results, as expected, the events are more compact than shallow earthquakes with the same magnitude (see the comparison with estimates assuming the scaling law of Wells and Coppersmith (1994) for shallow events in Figure S39 of Supporting Information S1). When accounting for the increase of rigidity with depth the source dimensions get close to the values expected for shallow events (Figure S41 in Supporting Information S1, bottom). Thus, similar to our findings for source duration, the increase of rigidity with depth can explain the differences in source dimensions between shallow and deep events. Moreover, we did not find again any clear dependency of the source spatial dimensions on depth.

In this study, we focus on the duration and spatial dimensions (A_{max} and A_{min}), which are generally well determined (Figures S9, S15, S19, S23, S27, S31, S35, and S39 in Supporting Information S1), but we also invert for the instantaneous spatial centroid velocity ($\mathbf{v_0}$). $\mathbf{v_0}$ is less well constrained in all inversions, but does not influence the recovery of other parameters (e.g., Figure S10 in Supporting Information S1). The error on $\mathbf{v_0}$ limits our ability to interpret the rupture velocity, or determine the directivity of these events using the directivity ratio (Section 1.3, Figure S40 in Supporting Information S1), but this is not the focus of this study.

The stress drops for all events are broadly in the range of ∼1–10 MPa (Figure 3), similar to the ranges reported by Poli et al. (2016), and the same order of magnitude as for shallow events (Allmann & Shearer, 2009). Similar to the results for source duration and spatial dimensions, they do not show any depth dependency. For well constrained events, such as event G or H, the stress drop estimates for all source models within 5% of the lowest misfit value are within an order of magnitude. Further, other events also have examples of source models with a fixed aspect ratio with stress drop error >5 MPa (e.g., Event B, sub-horizontal fault plane).

A notable event in our study region is the 2013 M_w 8.3 Okhotsk deep earthquake (∼611 km depth), which is the largest magnitude deep earthquake on record and has been investigated in detail by several previous studies (Chen et al., 2014; Park & Ishii, 2015; Steblov et al., 2014; Wei et al., 2013; Ye et al., 2013). We use the spatial extents reported by these studies to estimate the stress drop $\Delta\sigma$. Estimates range from ∼1 MPa (using the spatial extent of Ye et al. (2013)) to ∼12 MPa (using the spatial extent of Chen et al., 2014), which is in the same order of magnitude as the stress drops determined in this study. Therefore, we suggest that the rupture behavior of the 2013 M_w 8.3 Okhotsk earthquake is similar to that of the events in this study.

We obtain estimates of radiated energy in the range of $E_R \sim 10^{14}$–10^{16}J and moment-scaled energy E_R/M_0 in the range 7.9×10^{-6}–5.4×10^{-5} (Figure 3), which are in the same order as in other studies of deep earthquakes (Poli & Prieto, 2016; Ye et al., 2013). These estimates are a lower bound on the true radiated energy; some radiated energy may be missed if it is above the 0.5 Hz cut-off used for the SCARDEC source time functions, or lost due to unmodeled attenuation (Chounet & Vallée, 2018; Denolle & Shearer, 2016). For the shortest duration event in this study this could be up to 30% (Chounet & Vallée, 2018). On the other hand, we find many solutions for which the apparent radiation efficiency (Equation 2) is greater than one, which are not consistent with classical crack models. Such large estimates of efficiency are however not physically unrealistic: they imply stress undershooting, whereby the final stress on the fault is larger than the dynamic strength during slip.

The large efficiency values obtained are a result of the relatively low stress drops found in this study, and would remain even with the larger true radiated energy. These low stress drops are due to larger fault areas than in some previous studies. For example, Liu et al. (2020) observed moderate magnitude deep earthquakes with maximum spatial extents as small as ∼10 km. To confirm whether the larger spatial extents determined in this study are not a result of constraints of $A_{min} > 5$ km, we performed additional source inversions with the constraint $A_{min} > 10$ km and $A_{min} > 2.5$ km. The constraint $A_{min} > 10$ km led to A_{min} values consistent with those found with the constraint $A_{min} > 5$ km or to unstable inversion results (see Figure S40 in the Supporting Information S1). Similar behavior was observed with the constraint $A_{min} > 2.5$ km.

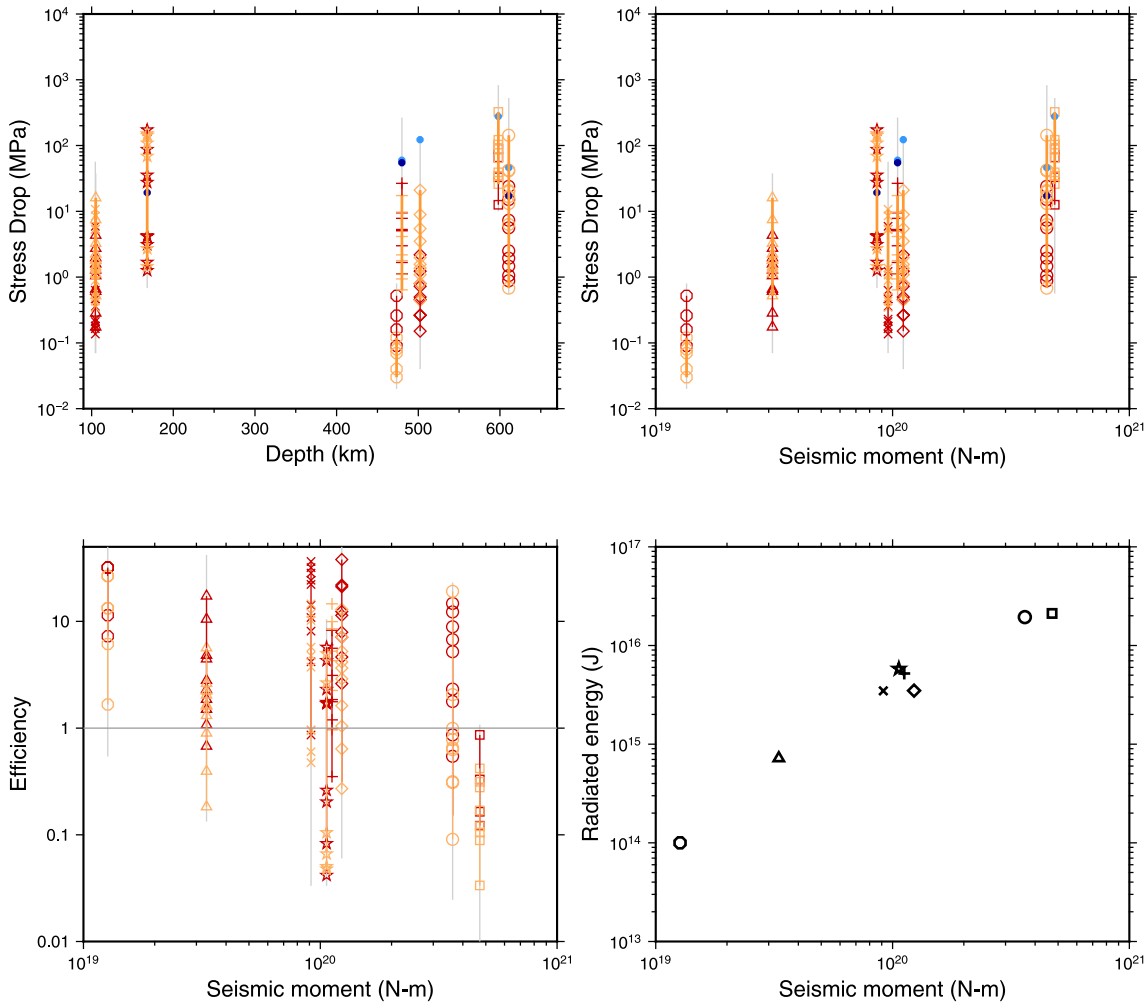

Figure 3. Top: Range of stress drops for each event versus depth (left) and seismic moment (right). Each event is represented by a different symbol (A: plus; B: circle; C: diamond; D: star; E: triangle; F: cross; G: octagon; H: square; see the corresponding source parameters in Table S1 in the Supporting Information S1). Dark and light blue circles are stress drop estimates from Poli and Prieto (2016) and Liu et al. (2020), respectively. Orange and red symbols correspond to solutions obtained assuming sub-vertical and sub-horizontal fault planes, respectively. Bottom: Range of apparent radiation efficiency (left) and radiated energy (right) versus seismic moment obtained in this study. Gray lines show model uncertainty, determined from all models within 5% of the minimum misfit.

Additionally, we test that our modeling approach does not systematically overestimate the spatial extent. To do so, we compare our $A_{\max}$ results to estimates of spatial extent using a fixed rupture speed (0.75 V_p; Poli & Prieto, 2016). We find that we do not systematically overestimate the rupture extent compared to this commonly used method. Since Liu et al. (2020) used a corner frequency approach based on higher frequency data than in this study, we suggest that they may have only observed a small patch of the rupture and determined high local stress drops. On the other hand, the lower frequency data used in this study provides constraints on the overall source process and a spatially averaged stress drop.

While Ye et al. (2013) also obtained many solutions with radiation efficiency larger than one for the Mw 8.3 Okhotsk event (~611 km depth), Tibi et al. (2003) and Poli et al. (2016) reported much lower efficiency values. Despite using distinct modeling approaches, both these studies were based on data with frequency higher than in this study, and hence may have only captured a small part of the whole rupture process, leading to high stress drops and low efficiencies.

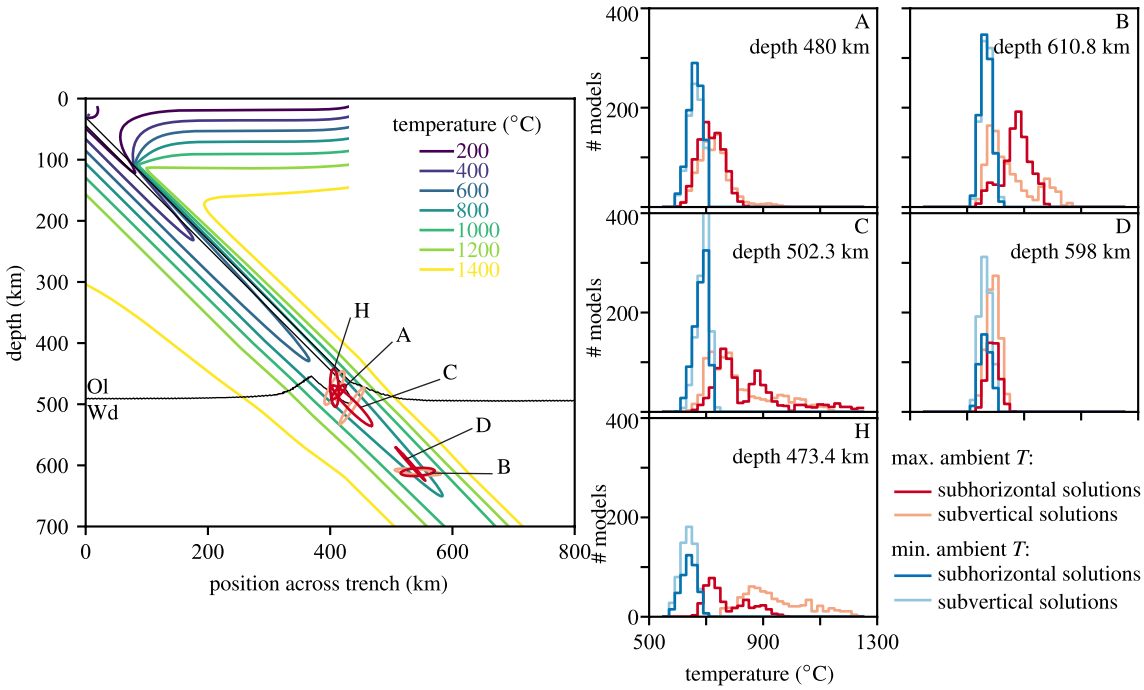

Figure 4. Left: Projection of the fault dimensions obtained from the higher moments source inversions on the slab background temperature obtained from a typical 2-D thermo-kinematics subduction model (see full details in Section 2.1 of Supporting Information S1; this example was computed using a plate velocity of 7 cm/year, dip angle of 40° and plate age of 75 Ma). The solutions corresponding to sub-horizontal fault planes are shown in dark red while sub-vertical fault plane solutions are shown in light red. Events E, F and G are not shown because they have a depth shallower than 200 km, for which the corner flow used in the modeling is limited (see full details in the Supporting Information S1). Right: Histograms showing the minimum and maximum temperatures crossed by the fault solutions at various depths for a range of subduction zone parameters, with subduction velocity ranging from 7.0 to 8.5 cm/year, plate dip angle from 40 to 50° and incoming lithosphere age from 75 to 85 Ma.

3. Thermal Modeling

In order to obtain a first-order estimate of the background temperature in the source region, we project the source dimensions obtained from the 20 inversions performed for each event into the temperature fields of a series of 2-D kinematic subduction thermal models. The models were obtained using two complementary approaches: (a) a computationally fast technique based on a simple slab geometry with added corner flow, which allows us to explore systematically the effect of slab dip angle, plate age and speed of subduction on the models (Davis, 2017); and, (b) a computationally more expensive mixed Eulerian-Lagrangian finite difference scheme enabling a more detailed representation of the slab geometry (Gerya & Yuen, 2003, see the Supporting Information S1 for further details about the subduction models used). Figure 4 and Figure S5 in Supporting Information S1 both show that while all earthquakes have relatively compact spatial dimensions, they propagate across the slab and beyond the slab's cold core. Previous studies suggested that if it exists, the MOW in cold, old slabs such as in the Kuril subduction zone should be around ~5–15 km and not exceed ~40 km (Kirby et al., 1996), which is smaller than the typical fault dimensions found in this study. Hence, our results are not compatible with a pure transformational faulting mechanism being responsible for both the triggering and propagation of deep earthquakes. Moreover, the majority of possible thermal fields, such as the one illustrated in Figure 4, suggest that a possible MOW (defined by ~600°C) would not reach the depth of the deepest events, ruling out transformational faulting as being responsible for them. As discussed previously, we do not find a depth trend in our results and while some events occur below the MOW, they appear to behave in the same way as their shallower counterparts. Similar to shallow earthquakes, the events are mostly confined in regions with temperature lower than ~1, 000°C (Figure 4, right; Figure S5 in Supporting Information S1), except for a few solutions for events C and H, which reach ~1, 300°C. Hence, the ruptures are mostly confined in regions with relatively low temperature where stress is potentially highest, suggesting that, similar to shallow earthquakes, background stress exerts a first order control on the propagation of deep earthquakes regardless of their nucleation mechanisms.

4. Mechanism and Propagation of Deep Earthquakes

Our estimates of stress drop and radiated energy result in high apparent radiation efficiency, which is the signature of the combination of large dynamic strength drops and small static stress drops (Noda et al., 2013). This situation typically arises if the rupture propagates as a self-healing slip pulse rather than as a crack (Heaton, 1990; Lambert et al., 2021). Earthquake propagation as self-healing pulses is characteristic of low ambient stress conditions and strong rate weakening friction (Gabriel et al., 2012; Zheng & Rice, 1998), and involves some degree of re-strengthening as slip arrests: dynamic fault strength is thus lower than the final static stress, which is also termed undershooting. To maintain the true radiation efficiency (ratio of radiated energy over available strain energy) below the theoretical upper limit of 1, stress undershoot must be greater than $\Delta\sigma(\eta_{app} - 1)/2$, which can be as high as 10 times the stress drop itself for our upper bounds of η_{app} (Figure 3). However, considering the rather low stress drops observed, such stress undershoots are not necessarily physically unrealistic. Laboratory high velocity friction experiments have indeed shown that dynamic fault strength is extremely low at high deformation rate, and exhibits significant strengthening as slip stops (Violay et al., 2019). Such a behavior is typically due to the strong rate-dependence of the viscous flow mechanisms at play, possibly grain-size sensitive creep (Pozzi et al., 2021) or viscous deformation of the melt layer when melting occurs (Hirose & Shimamoto, 2005), and transient relative cooling of the shear zone as slip decelerates (Proctor et al., 2014). Under the extreme ambient pressure at the source of deep earthquakes, sudden textural changes and mineral transformations have been evidenced experimentally (Green et al., 2015). They are expected to produce high strain rheology consistent with that observed at lower pressure (in the laboratory) and required by our estimates of radiated energy and stress drop.

In addition to the intrinsic rheology of the fault the ambient stress distribution along the fault plane likely contributes to the low stress drop and high radiation efficiency. Our thermomechanical models reveal that ambient temperature is likely high at the edges of the fault, so that the local stress state is also probably low due to long-term creep in those regions. We therefore expect that earthquakes initiate in the cold core of the slab, where significant elastic stress can be maintained, and then propagate outwards into warmer regions where stress is low: the stress drop might be locally large near the nucleation patch, but could become gradually zero or locally negative as rupture propagates, leading to a small spatially averaged stress drop (Noda et al., 2013).

Taken together, our observations and model results indicate that deep earthquakes may initiate in the cold, MOW of the downgoing slab, but most certainly propagate beyond that region into warmer, low stress environment, which could be responsible for their arrest (Billen, 2020). Regardless of the nucleation mechanism, which could well be transformational faulting, propagation is therefore most certainly driven by viscous weakening mechanisms, such as grain-size sensitive creep or flow of a melt layer, which could be similar to those driving shallow ruptures (Hirose & Shimamoto, 2005; Pozzi et al., 2021). Such mechanisms are consistent with the low stress drops and large radiated energy inferred from the seismological data. Overall, the source properties of the deep earthquakes analyzed here do not appear to be significantly different from those of regular earthquakes of similar magnitudes.

Data Availability Statement

All source models are available in the Supporting Information S1 or in csv format at https://doi.org/10.5281/zenodo.6279848.

Acknowledgments
The authors thank the editor Germán Prieto, and reviewers Piero Poli and an anonymous reviewer for their valuable reviews, which greatly helped improve this manuscript. We gratefully acknowledge the availability of global seismograms from the IRIS Data Services and the II, IU, GEOSCOPE and GEOFON networks. The seismic waveform modeling carried out on the High Performance Computing Cluster supported by the Research and Computing Support services at University College London and on the national UK supercomputing facility Archer. We thank Martin Vallée, Hiroo Kanamori and Michael Frietsch for fruitful discussions. This research was supported by NERC grant NE/N011791/1.

References

Allmann, B. P., & Shearer, P. M. (2009). Global variations of stress drop for moderate to large earthquakes. *Journal of Geophysical Research*, *114*(B1), B01310. https://doi.org/10.1029/2008JB005821

Antolik, M., Dreger, D., & Romanowicz, B. (1999). Rupture processes of large deep-focus earthquakes from inversion of moment rate functions. *Journal of Geophysical Research*, *104*(B1), 863–894. https://doi.org/10.1029/1998jb900042

Backus, G. E. (1977a). Interpreting the seismic glut moments of total degree two or less. *Geophysical Journal International*, *51*(1), 1–25. https://doi.org/10.1111/j.1365-246x.1977.tb04187.x

Backus, G. E. (1977b). Seismic sources with observable glut moments of spatial degree two. *Geophysical Journal International*, *51*(1), 27–45. https://doi.org/10.1111/j.1365-246x.1977.tb04188.x

Bassin, C. (2000). The current limits of resolution for surface wave tomography in North America. *EOS Transactions American Geophysical Union*, *81*, 29.

Bilek, S., Lay, T., & Ruff, L. (2004). Radiated seismic energy and earthquake source duration variations from teleseismic source time functions for shallow subduction zone thrust earthquakes. *Journal of Geophysical Research*, *109*(B9), B09308. https://doi.org/10.1029/2004jb003039

Billen, M. I. (2020). Deep slab seismicity limited by rate of deformation in the transition zone. *Science Advances*, *6*(22), eaaz7692. https://doi.org/10.1126/sciadv.aaz7692

Campus, P., & Das, S. (2000). Comparison of the rupture and radiation characteristics of intermediate and deep earthquakes. *Journal of Geophysical Research*, *105*(B3), 6177–6189. https://doi.org/10.1029/1999jb900384

Chang, S.-J., Ferreira, A. M., Ritsema, J., van Heijst, H. J., & Woodhouse, J. H. (2015). Joint inversion for global isotropic and radially anisotropic mantle structure including crustal thickness perturbations. *Journal of Geophysical Research: Solid Earth*, *120*(6), 4278–4300. https://doi.org/10.1002/2014jb011824

Chen, Y., Wen, L., & Ji, C. (2014). A cascading failure during the 24 May 2013 great Okhotsk deep earthquake. *Journal of Geophysical Research: Solid Earth*, *119*(4), 3035–3049. https://doi.org/10.1002/2013jb010926

Chounet, A., & Vallée, M. (2018). Global and interregion characterization of subduction interface earthquakes derived from source time functions properties. *Journal of Geophysical Research: Solid Earth*, *123*(7), 5831–5852. https://doi.org/10.1029/2018jb015932

Clévédé, E., Bouin, M.-P., Bukchin, B., Mostinskiy, A., & Patau, G. (2004). New constraints on the rupture process of the 1999 August 17 Izmit earthquake deduced from estimates of stress glut rate moments. *Geophysical Journal International*, *159*(3), 931–942. https://doi.org/10.1111/j.1365-246x.2004.02304.x

Courboulex, F., Vallée, M., Causse, M., & Chounet, A. (2016). Stress-drop variability of shallow earthquakes extracted from a global database of source time functions. *Seismological Research Letters*, *87*(4), 912–918. https://doi.org/10.1785/0220150283

Davies, J. H. (1999). The role of hydraulic fractures and intermediate-depth earthquakes in generating subduction-zone magmatism. *Nature*, *398*(6723), 142–145. https://doi.org/10.1038/18202

Davis, P. M. (2017). Dependence of the brittle ductile transition on strain-rate-dependent critical homologous temperature. *Geophysical Journal International*, *209*, 1180–1194.

Denolle, M. A. (2019). Energetic onset of earthquakes. *Geophysical Research Letters*, *46*(5), 2458–2466. https://doi.org/10.1029/2018gl080687

Denolle, M. A., & Shearer, P. M. (2016). New perspectives on self-similarity for shallow thrust earthquakes. *Journal of Geophysical Research: Solid Earth*, *121*(9), 6533–6565. https://doi.org/10.1002/2016jb013105

Ekström, G., Nettles, M., & Dziewoński, A. (2012). The global CMT project 2004–2010: Centroid-moment tensors for 13, 017 earthquakes. *Physics of the Earth and Planetary Interiors*, *200*, 1–9. https://doi.org/10.1016/j.pepi.2012.04.002

Engdahl, E. R., van der Hilst, R., & Buland, R. (1998). Global teleseismic earthquake relocation with improved travel times and procedures for depth determination. *Bulletin of the Seismological Society of America*, *88*(3), 722–743.

Eshelby, J. D. (1957). The determination of the elastic field of an ellipsoidal inclusion, and related problems. *Proceedings of the Royal Society of London, Series A: Mathematical and Physical Sciences*, *241*(1226), 376–396.

Fan, W., Wei, S. S., Tian, D., McGuire, J. J., & Wiens, D. A. (2019). Complex and diverse rupture processes of the 2018 M w 8.2 and M w 7.9 Tonga-Fiji deep earthquakes. *Geophysical Research Letters*, *46*(5), 2434–2448. https://doi.org/10.1029/2018gl080997

Fukao, Y., & Obayashi, M. (2013). Subducted slabs stagnant above, penetrating through, and trapped below the 660 km discontinuity. *Journal of Geophysical Research*, *118*(11), 5920–5938. https://doi.org/10.1002/2013JB010466

Gabriel, A.-A., Ampuero, J.-P., Dalguer, L. A., & Mai, P. M. (2012). The transition of dynamic rupture styles in elastic media under velocity-weakening friction. *Journal of Geophysical Research*, *117*(B9), B09311. https://doi.org/10.1029/2012JB009468

Gerya, T., & Yuen, D. A. (2003). Characteristics-based marker-in-cell method with conservative finite-differences schemes for modeling geological fows with strongly variable transport properties. *Physics of the Earth and Planetary Interiors*, *140*(4), 293–318. https://doi.org/10.1016/j.pepi.2003.09.006

Green, H. W., Shi, F., Bozhilov, K., Xia, G., & Reches, Z. (2015). Phase transformation and nanometric flow cause extreme weakening during fault slip. *Nature Geoscience*, *8*(6), 484–489. https://doi.org/10.1038/ngeo2436

Heaton, T. H. (1990). Evidence for and implications of self-healing pulses of slip in earthquake rupture. *Physics of the Earth and Planetary Interiors*, *64*, 1–20. https://doi.org/10.1016/0031-9201(90)90002-f

Hirose, T., & Shimamoto, T. (2005). Growth of molten zone as a mechanism of slip weakening of simulated faults in gabbro during frictional melting. *Journal of Geophysical Research*, *110*(B5), B05202. https://doi.org/10.1029/2004JB003207

Houston, H. (2015). 4.13—Deep earthquakes. In G. Schubert (Ed.), *Treatise on geophysics* (2nd ed., pp. 329–354). Elsevier. https://doi.org/10.1016/B978-0-444-53802-4.00079-8

Houston, H., Benz, H. M., & Vidale, J. E. (1998). Time functions of deep earthquakes from broadband and short-period stacks. *Journal of Geophysical Research*, *103*(B12), 29895–29913. https://doi.org/10.1029/98jb02135

Kirby, S. H., Stein, S., Okal, E. A., & Rubie, D. C. (1996). Metastable mantle phase transformations and deep earthquakes in subducting oceanic lithosphere. *Reviews of Geophysics*, *34*(2), 261–306. https://doi.org/10.1029/96rg01050

Kiser, E., Ishii, M., Langmuir, C. H., Shearer, P., & Hirose, H. (2011). Insights into the mechanism of intermediate-depth earthquakes from source properties as imaged by back projection of multiple seismic phases. *Journal of Geophysical Research*, *116*(B6), B06310. https://doi.org/10.1029/2010jb007831

Lambert, V., Lapusta, N., & Perry, S. (2021). Propagation of large earthquakes as self-healing pulses or mild cracks. *Nature*, *591*(7849), 252–258. https://doi.org/10.1038/s41586-021-03248-1

Liu, M., Huang, Y., & Ritsema, J. (2020). Stress drop variation of deep-focus earthquakes based on empirical Green's function.

McGuire, J. J., Zhao, L., & Jordan, T. H. (2001). Teleseismic inversion for the second degree moments of earthquake space–time distributions. *Geophysical Journal International*, *145*(3), 661–678. https://doi.org/10.1046/j.1365-246x.2001.01414.x

Meng, L., Ampuero, J.-P., & Bürgmann, R. (2014). The 2013 Okhotsk deep-focus earthquake: Rupture beyond the metastable olivine wedge and thermally controlled rise time near the edge of a slab. *Geophysical Research Letters*, *41*(11), 3779–3785. https://doi.org/10.1002/2014gl059968

Myhill, R. (2012). Slab buckling and its effect on the distributions and focal mechanisms of deep-focus earthquakes. *Geophysical Journal International*, *192*(2), 837–853. https://doi.org/10.1093/gji/ggs054

Noda, H., Lapusta, N., & Kanamori, H. (2013). Comparison of average stress drop measures for ruptures with heterogeneous stress change and implications for earthquake physics. *Geophysical Journal International*, *193*(3), 1691–1712. https://doi.org/10.1093/gji/ggt074

Ogawa, M. (1987). Shear instability in a viscoelastic material as the cause of deep focus earthquakes. *Journal of Geophysical Research*, *92*(B13), 13801–13810. https://doi.org/10.1029/jb092ib13p13801

Park, S., & Ishii, M. (2015). Inversion for rupture properties based upon 3-D directivity effect and application to deep earthquakes in the Sea of Okhotsk region. *Geophysical Journal International*, *203*(2), 1011–1025. https://doi.org/10.1093/gji/ggv352

Poli, P., & Prieto, G. (2014). Global and along-strike variations of source duration and scaling for intermediate-depth and deep-focus earthquakes. *Geophysical Research Letters*, *41*(23), 8315–8324. https://doi.org/10.1002/2014gl061916

Poli, P., Prieto, G., Rivera, E., & Ruiz, S. (2016). Earthquakes initiation and thermal shear instability in the Hindu Kush intermediate depth nest. *Geophysical Research Letters*, *43*(4), 1537–1542. https://doi.org/10.1002/2015gl067529

Poli, P., & Prieto, G. A. (2016). Global rupture parameters for deep and intermediate-depth earthquakes. *Journal of Geophysical Research: Solid Earth*, *121*(12), 8871–8887. https://doi.org/10.1002/2016jb013521

Pozzi, G., De Paola, N., Nielsen, S., Holdsworth, R. E., Tesei, T., Thieme, M., & Demouchy, S. (2021). Coseismic fault lubrication by viscous deformation. *Nature Geoscience*, *14*(6), 437–442. https://doi.org/10.1038/s41561-021-00747-8

Proctor, B. P., Mitchell, T. M., Hirth, G., Goldsby, D., Zorzi, F., Platt, J. D., & Di Toro, G. (2014). Dynamic weakening of serpentinite gouge and bare-surfaces at seismic slip rates. *Journal of Geophysical Research*, *119*(11), 8107–8131. https://doi.org/10.1002/2014JB011057

Ruiz, S., Tavera, H., Poli, P., Herrera, C., Flores, C., Rivera, E., & Madariaga, R. (2017). The deep Peru 2015 doublet earthquakes. *Earth and Planetary Science Letters*, *478*, 102–109. https://doi.org/10.1016/j.epsl.2017.08.036

Sambridge, M. (1999). Geophysical inversion with a neighbourhood algorithm– i. searching a parameter space. *Geophysical Journal International*, *138*(2), 479–494. https://doi.org/10.1046/j.1365-246x.1999.00876.x

Steblov, G. M., Ekström, G., Kogan, M. G., Freymueller, J. T., Titkov, N. N., Vasilenko, N. F., et al. (2014). First geodetic observations of a deep earthquake: The 2013 Sea of Okhotsk Mw 8.3, 611 km-deep, event. *Geophysical Research Letters*, *41*(11), 3826–3832. https://doi.org/10.1002/2014gl060003

Syracuse, E. M., & Abers, G. A. (2006). Global compilation of variations in slab depth beneath arc volcanoes and implications. *Geochemistry, Geophysics, Geosystems*, *7*(5), Q05017. https://doi.org/10.1029/2005gc001045

Syracuse, E. M., van Keken, P. E., & Abers, G. A. (2010). The global range of subduction zone thermal models. *Physics of the Earth and Planetary Interiors*, *183*(1–2), 73–90. https://doi.org/10.1016/j.pepi.2010.02.004

Tibi, R., Bock, G., & Wiens, D. A. (2003). Source characteristics of large deep earthquakes: Constraint on the faulting mechanism at great depths. *Journal of Geophysical Research*, *108*(B2), 2091. https://doi.org/10.1029/2002JB001948

Vallée, M. (2013). Source time function properties indicate a strain drop independent of earthquake depth and magnitude. *Nature Communications*, *4*(1), 2606. https://doi.org/10.1038/ncomms3606

Vallée, M., Charléty, J., Ferreira, A. M., Delouis, B., & Vergoz, J. (2011). SCARDEC: A new technique for the rapid determination of seismic moment magnitude, focal mechanism and source time functions for large earthquakes using body-wave deconvolution. *Geophysical Journal International*, *184*(1), 338–358. https://doi.org/10.1111/j.1365-246x.2010.04836.x

Vallée, M., & Douet, V. (2016). A new database of source time functions (STFs) extracted from the SCARDEC method. *Physics of the Earth and Planetary Interiors*, *257*, 149–157. https://doi.org/10.1016/j.pepi.2016.05.012

Vassiliou, M., & Kanamori, H. (1982). The energy release in earthquakes. *Bulletin of the Seismological Society of America*, *72*, 371–387.

Venkataraman, A., & Kanamori, H. (2004). Observational constraints on the fracture energy of subduction zone earthquakes. *Journal of Geophysical Research*, *109*(B5), B05302. https://doi.org/10.1029/2003JB002549

Vidale, J. E., & Houston, H. (1993). The depth dependence of earthquake duration and implications for rupture mechanisms. *Nature*, *365*(6441), 45–47. https://doi.org/10.1038/365045a0

Violay, M., Passelègue, F., Spagnuolo, E., Di Toro, G., & Cornelio, C. (2019). Effect of water and rock composition on re-strengthening of cohesive faults during the deceleration phase of seismic slip pulses. *Earth and Planetary Science Letters*, *522*, 55–64. https://doi.org/10.1016/j.epsl.2019.06.027

Wang, Y., Zhu, L., Shi, F., Schubnel, A., Hilairet, N., Yu, T., et al. (2017). A laboratory nanoseismological study on deep-focus earthquake micromechanics. *Science Advances*, *3*(7), e1601896. https://doi.org/10.1126/sciadv.1601896

Warren, L. M., Baluyut, E. C., Osburg, T., Lisac, K., & Kokkinen, S. (2015). Fault plane orientations of intermediate-depth and deep-focus earthquakes in the Japan-Kuril-Kamchatka subduction zone. *Journal of Geophysical Research: Solid Earth*, *120*(12), 8366–8382. https://doi.org/10.1002/2015jb012463

Warren, L. M., Hughes, A. N., & Silver, P. G. (2007). Earthquake mechanics and deformation in the Tonga-Kermadec subduction zone from fault plane orientations of intermediate-and deep-focus earthquakes. *Journal of Geophysical Research*, *112*(B5), B05314. https://doi.org/10.1029/2006jb004677

Warren, L. M., Langstaff, M. A., & Silver, P. G. (2008). Fault plane orientations of intermediate-depth earthquakes in the Middle America Trench. *Journal of Geophysical Research*, *113*(B1), B01304. https://doi.org/10.1029/2007jb005028

Wei, S., Helmberger, D., Zhan, Z., & Graves, R. (2013). Rupture complexity of the mw 8.3 sea of okhotsk earthquake: Rapid triggering of complementary earthquakes? *Geophysical Research Letters*, *40*(19), 5034–5039. https://doi.org/10.1002/grl.50977

Wells, D. L., & Coppersmith, K. J. (1994). New empirical relationships among magnitude, rupture length, rupture width, rupture area, and surface displacement. *Bulletin of the Seismological Society of America*, *84*(4), 974–1002.

Ye, L., Lay, T., Kanamori, H., & Koper, K. D. (2013). Energy release of the 2013 Mw 8.3 Sea of Okhotsk earthquake and deep slab stress heterogeneity. *Science*, *341*(6152), 1380–1384. https://doi.org/10.1126/science.1242032

Ye, L., Lay, T., Kanamori, H., Zhan, Z., & Duputel, Z. (2016). Diverse rupture processes in the 2015 Peru deep earthquake doublet. *Science Advances*, *2*(6), e1600581. https://doi.org/10.1126/sciadv.1600581

Zhan, Z. (2019). Mechanisms and implications of deep earthquakes. *Annual Review of Earth and Planetary Sciences*, *48*(1), 147–174. https://doi.org/10.1146/annurev-earth-053018-060314

Zhan, Z., Kanamori, H., Tsai, V. C., Helmberger, D. V., & Wei, S. (2014). Rupture complexity of the 1994 Bolivia and 2013 sea of Okhotsk deep earthquakes. *Earth and Planetary Science Letters*, *385*, 89–96. https://doi.org/10.1016/j.epsl.2013.10.028

Zheng, G., & Rice, J. R. (1998). Conditions under which velocity-weakening friction allows a self-healing versus a cracklike more of rupture. *Bulletin of the Seismological Society of America*, *88*(6), 1466–1483.